Supporting Information

Electrocatalytic hydrogen evolution in neutral pH solutions: dual phase synergy

*Xiaohong Xie, Miao Song, Luguang Wang, Mark H. Engelhard, Langli Luo, Andrew Miller, Yayun Zhang, Lei Du, Huilin Pan, Zimin Nie, Yuanyuan Chu, Luis Estevez, Zidong Wei, Hong Liu, Chongmin Wang, Dongsheng Li, and Yuyan Shao**

Dr. X. Xie, Dr. M. Song, Dr. M. H. Engelhard, Dr. L. Luo, Dr. L. Du, Dr. H. Pan, Dr. Z. Nie, Dr. Y. Chu, Dr. L. Estevez, Dr. C. Wang, Dr. Y. Shao.
Pacific Northwest National Laboratory, Richland, Washington 99352, United States
E-mail: yuyan.shao@pnnl.gov

L. Wang, A. Miller, Prof. H. Liu.
Department of Biological and Ecological Engineering, Oregon State University, Corvallis, 97331, United States

Prof. Z. Wei.
Chongqing Key Laboratory of Chemical Process for Clean Energy and Resource Utilization, School of Chemistry and Chemical Engineering, Chongqing University, Chongqing 400044, China

Dr. Y. Zhang
Bioproducts, Sciences and Engineering Laboratory, Department of Biological Systems Engineering, Washington State University, Richland, Washington 99352, United States

Figures S1-S12
Tables S1-S2

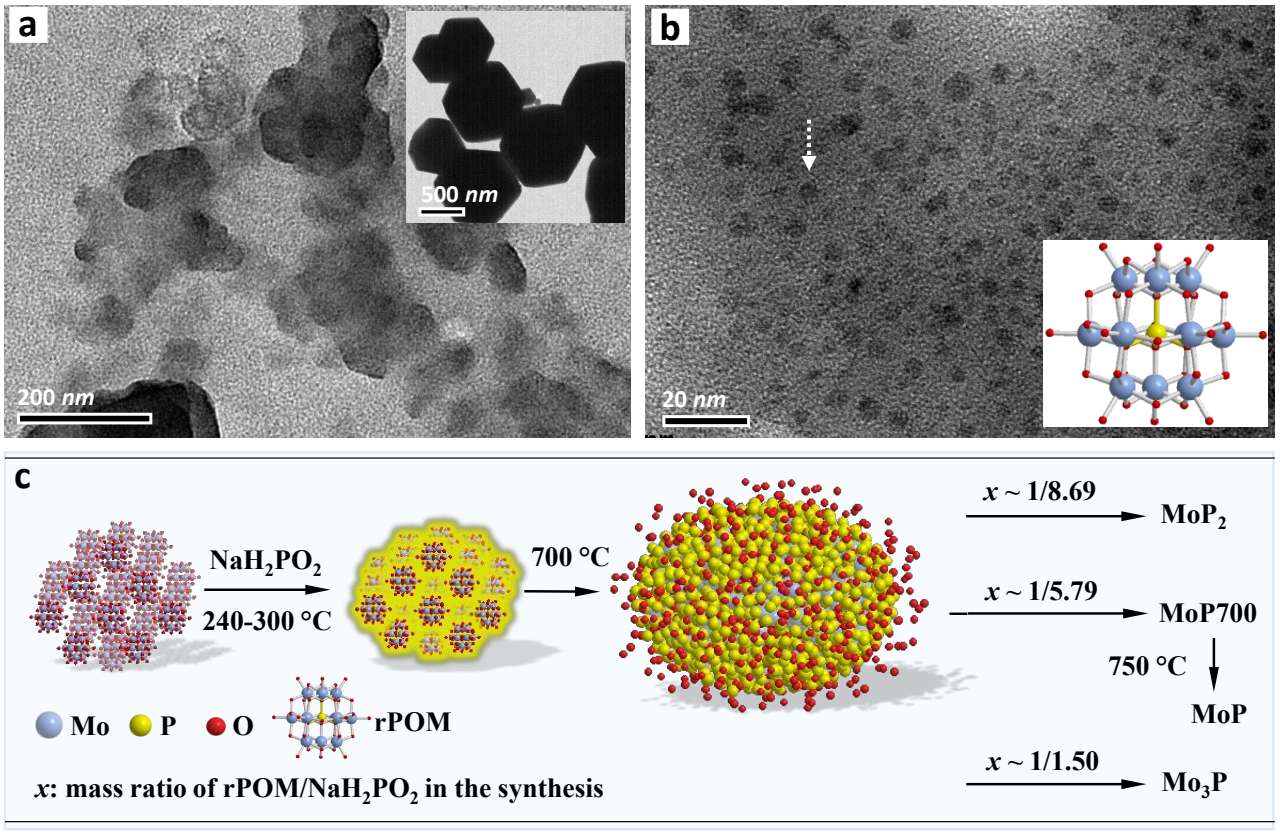

Figure S1.

TEM (a) and HRTEM (b) images of reduced POM (rPOM); inset (a): TEM image of $(NH_4)_3PMo_{12}O_{40}$. (c) Schematic diagram illustrates the synthesis process of MoP700, MoP, MoP_2 and Mo_3P.

The formation of MoP_x is strongly associated with the high thermal stability of the rPOM nanocluster, in which the steric structure can only be decomposed into atomic Mo reactants at temperatures near 700 °C. At lower temperatures, the nanocluster structure of rPOM can be maintained and the P or PH_3 species from the decomposition of NaH_2PO_2 (240-300 °C) could diffuse and then adsorb on the rPOM nanoclusters to form a solid composite consisting of rPOM encapsulated by P (rPOM@P). When the temperature is further increased to 700 °C, the rPOM is decomposed and Mo and P atoms immediately combine to form MoP_x. MoP700, MoP_2 and MoP were synthesized by adjust the mass ratio of rPOM and NaH_2PO_2 precursors.

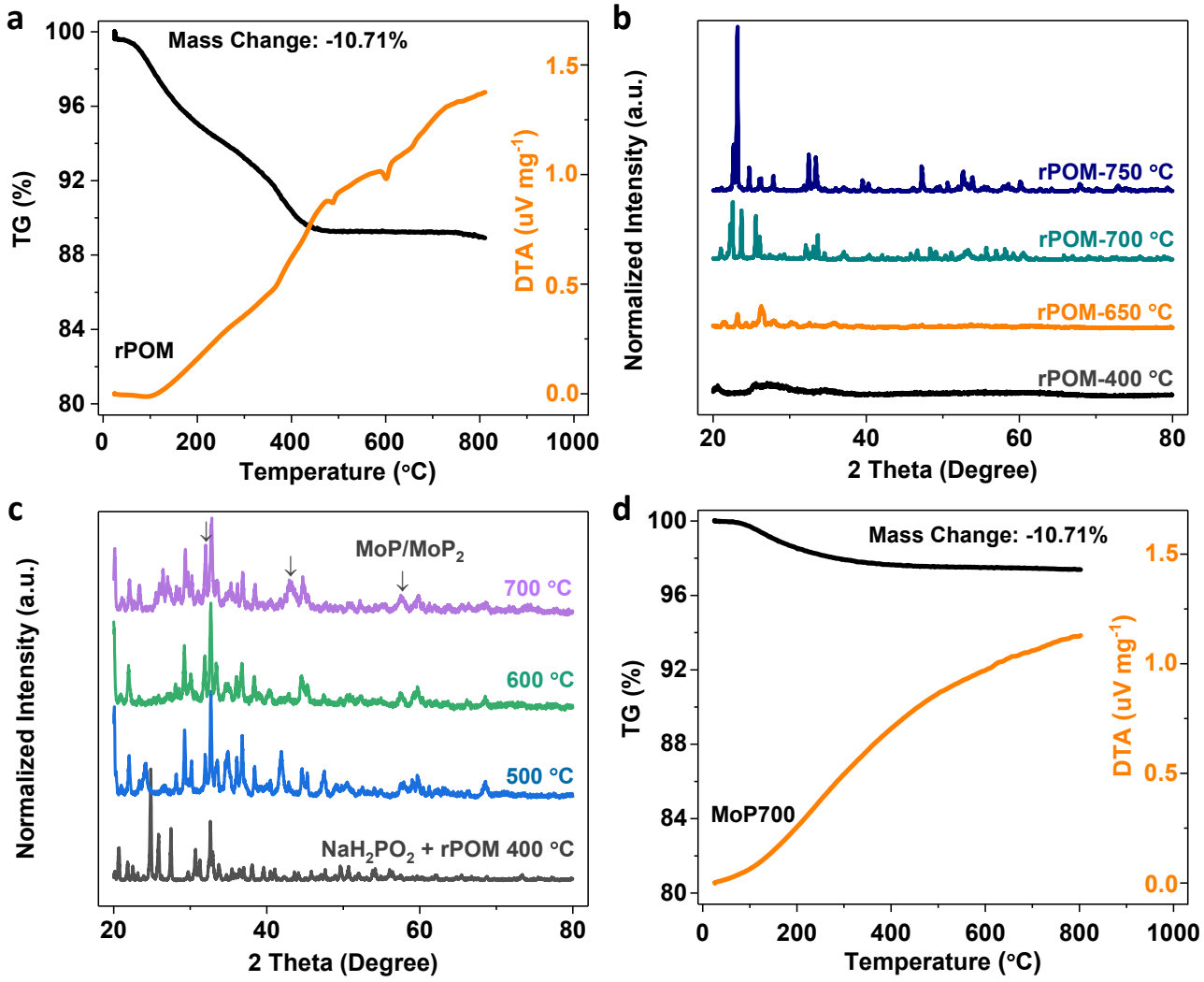

Figure S2.

(a) Thermogravimetric analysis (TGA) curves of rPOM. The sample had a 10.71 % mass loss by ~480 °C due to the loss of crystal H_2O. There is very little mass loss from 400-700 °C, confirming the rPOM precursor structure is stable. (b) XRD patterns for rPOM treated at different temperatures. (c) XRD patterns for rPOM and NaH_2PO_2 mixture treated at temperatures from 400 to 700 °C. Note that no MoP_x phases can be observed in products heated at temperatures below 700 °C, that is, no MoP_x was produced; when the conversion was subjected to 700 °C, the temperature supplied enough and suitable energy for the rPOM cluster decomposing and thus promoted the combination of Mo and P to form MoP. (d) TGA curves of MoP700.

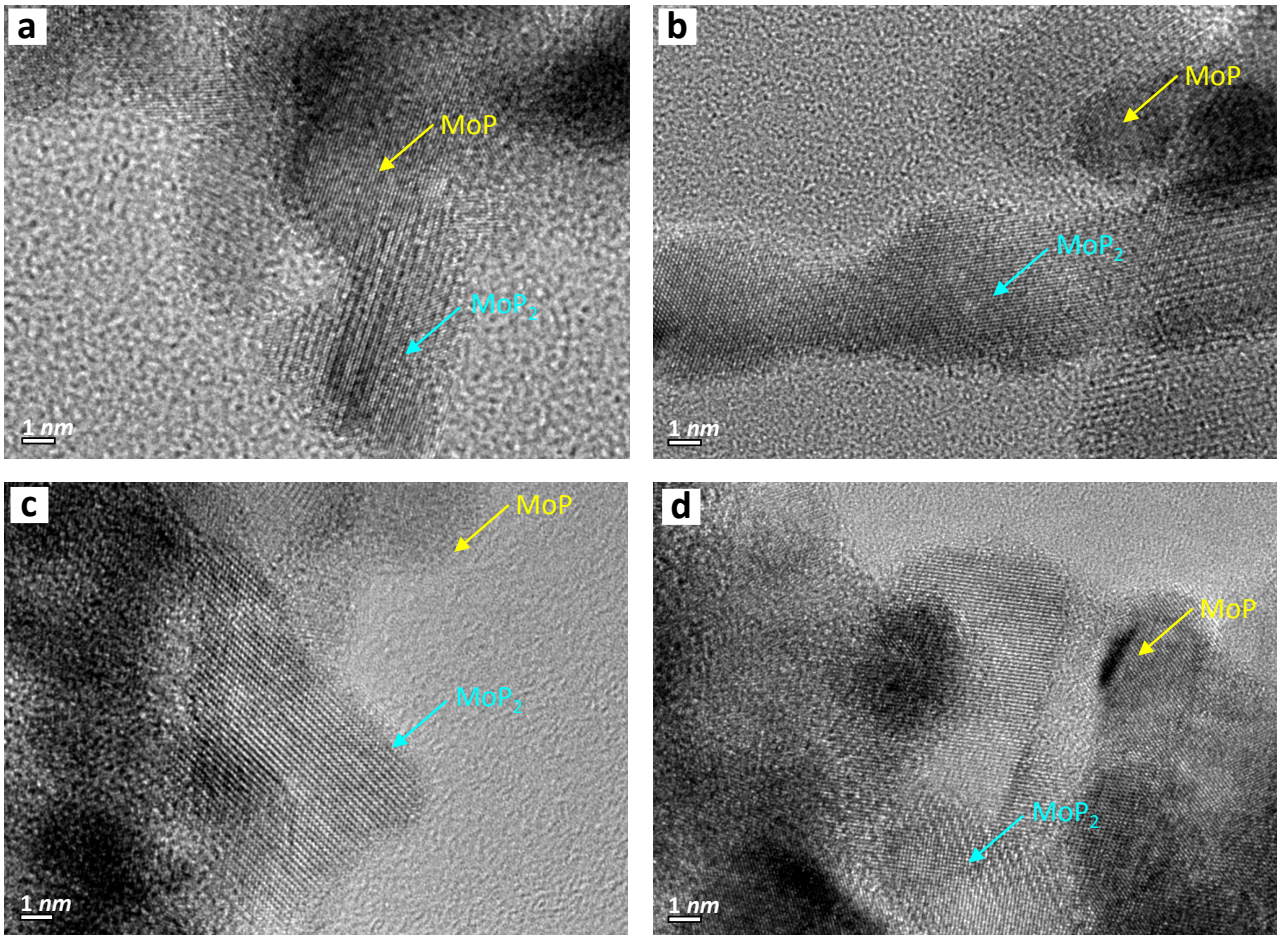

Figure S3.

(a-d) HRTEM images of MoP700 showing the coexistence of MoP and MoP_2 in the as-synthesized catalyst.

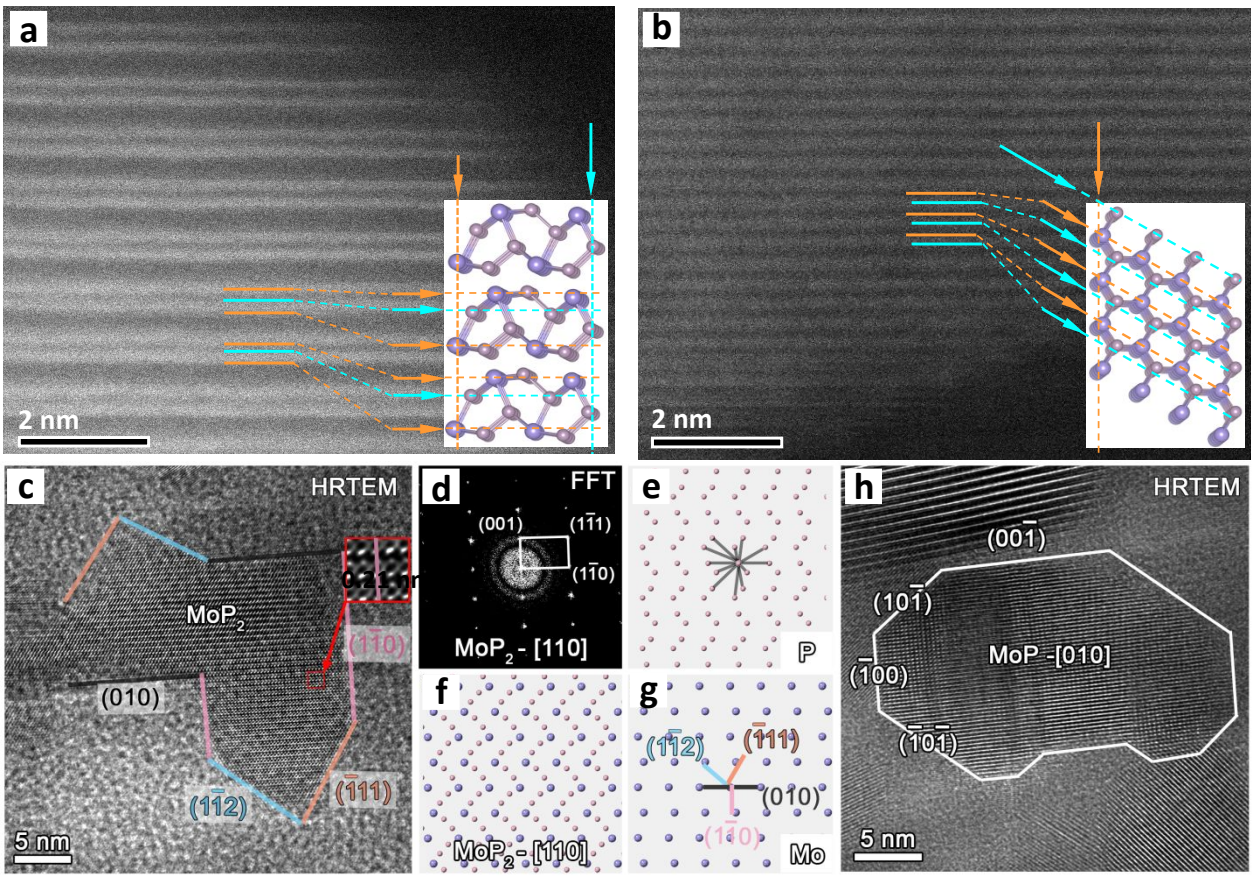

Figure S4.

HADDF-STEM images of typical (a) MoP_2 and (b) MoP phases in MoP700. (c) HRTEM image of a MoP_2 nanoparticle, the enlarged red-boxed area shows the detailed structure of (1-10) plane. Different surface facets were identified by solid colored lines. (d) FFT image of the MoP_2 particls. (e) Simulated crystal structure of MoP_2 along the [110] zone axis. (f) Distribution of P atoms along the [110] zone axis. (g) Distribution of Mo atoms along the [110] zone axis, several possible facets of Mo-terminated surfaces with lower Miller indices were identified by solid lines, which are consistent with surface facets identified in (c). (h) HRTEM image of a MoP nanoparticle along the [010] zone axis. Various surface facets were identified by white lines.

The HAADF-STEM image (Figure S4a) of typical MoP_2 exhibited a zigzagging layered structure and the Mo and P atoms are separated into 3 different columns. Because the contrast approximately scales with $Z^{1.7}$, the brighter columns correspond to Mo atoms and the interbedded lighter column is P atoms. Figure S4b shows the HAADF-STEM image of typical MoP phase oriented along the [001] direction in which the Mo and P atoms are separated in 2 different columns.[1-2] The brighter columns correspond to Mo atoms and the lighter ones correspond to P atoms. The bright edges of MoP phase indicate that the surface atoms can be identified as Mo; that is, MoP possesses Mo-terminated surface. Those result suggests that the outmost atomic layers of MoP and MoP_2 phases are Mo-terminated, as illustrated in inset Figure S4 a and b, respectively.

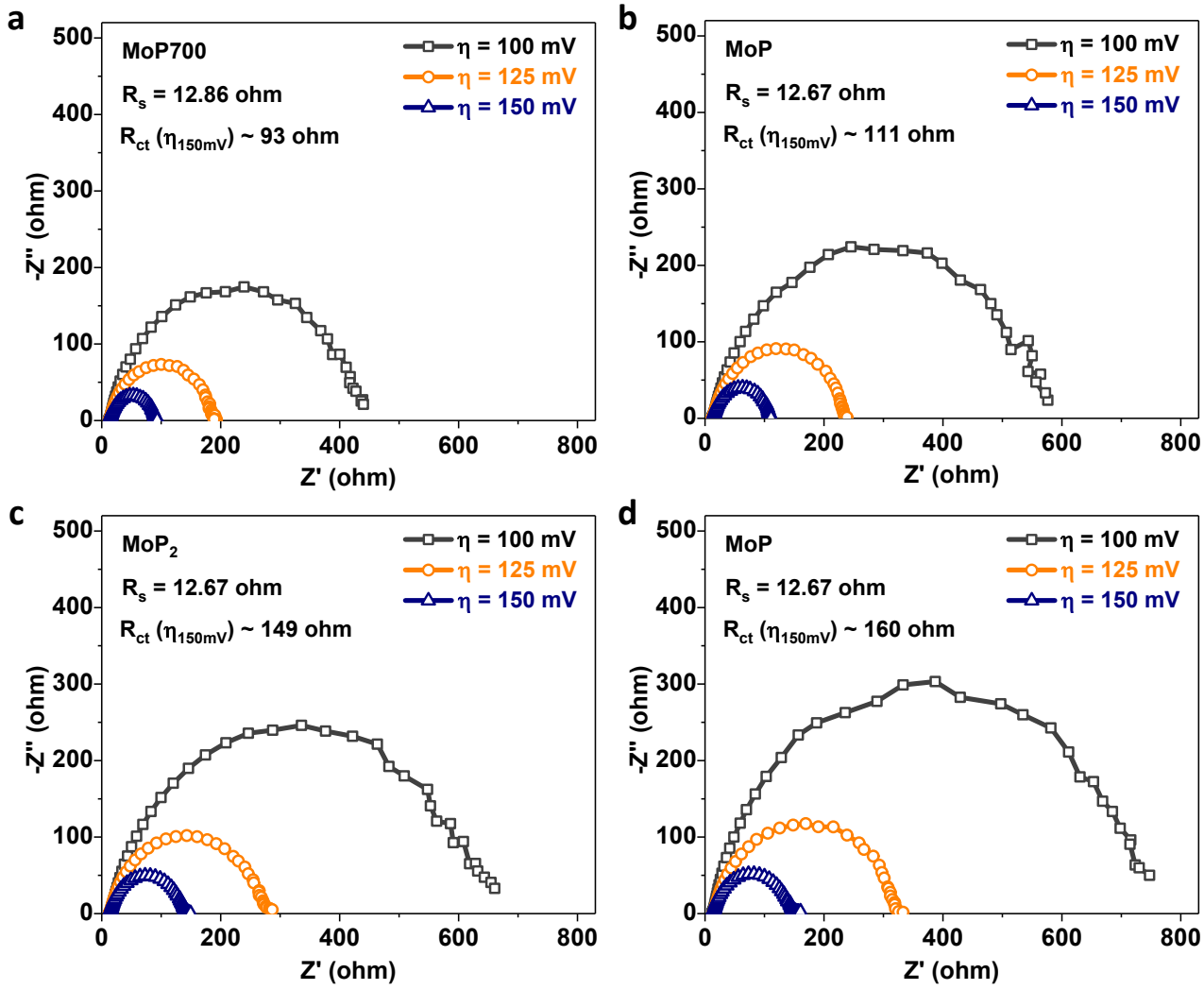

Figure S5.

Nyquist plots of (a) MoP700, (b) MoP, (c) MoP_2, and (d) Mo_3P at different overpotentials (η) from 100 to 150 mV.

All electrodes show small and similar series resistance (R_s), suggesting that the experimental setup was consistent. The slight variation of R_s in different electrodes can be attributed to the differences in electrode resistance. Basically, transition metal phosphides (e.g., MoP, Ni_2P, and Co_2P) have physical properties similar to those of ordinary metallic compounds like the carbides, nitrides, and borides. They combine the properties of metals and ceramics, and therefore exhibit metal-like properties and high electrical conductivity.[3-4]

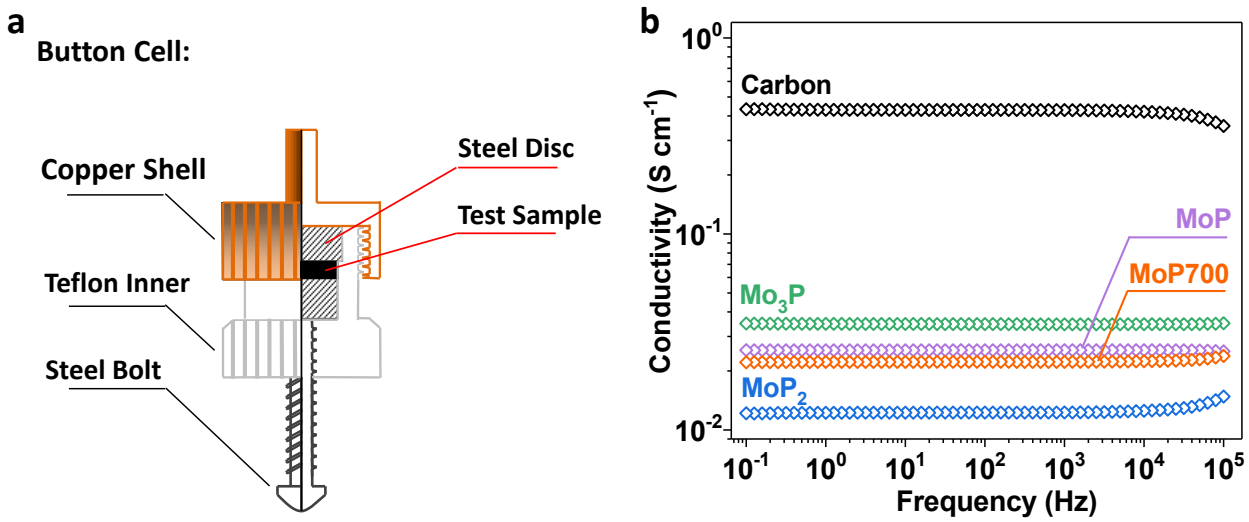

Figure S6.

(a) Illustration of the home-made button cell. (b) Electrical conductivity of MoP700, MoP, MoP_2 and Mo_3P in compared with conductive carbon.

Electrical conductivity measurement was performed using a home-made button cell by confining the catalyst between two smooth polished steel discs and measuring the electrical resistance of the sample by AC electric impedance spectroscopy. The operating frequency range was 0.1-100,000 Hz, the AC amplitude was 10 mV, and the DC potential was 0 V compared to an open circuit.A Solartron SI 1287 Electrochemical Interface and a Solartron SI 1260 Impedance/Gain-phase Analyzer coupling system was used.

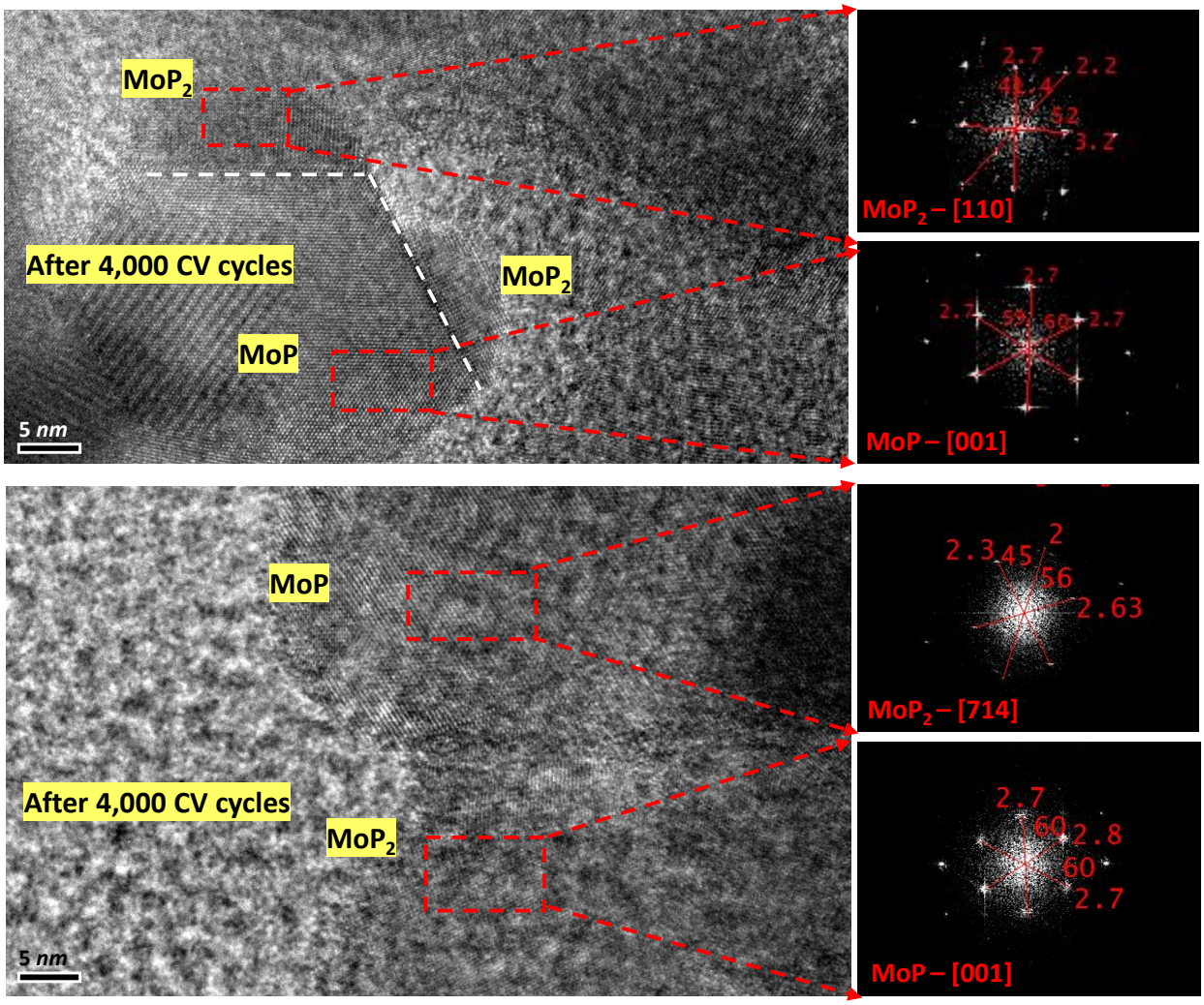

Figure S7.

HRTEM and FFT images of MoP700 after 4,000 CV cycles between -0.45 and 0.15 V vs RHE in H_2-saturated 1.0 M PBS, which clearly show the two phases of MoP/MoP_2, similar to the sample before the stability test (Fig.1b), indicating no obvious structure change for MoP700 during stability test.

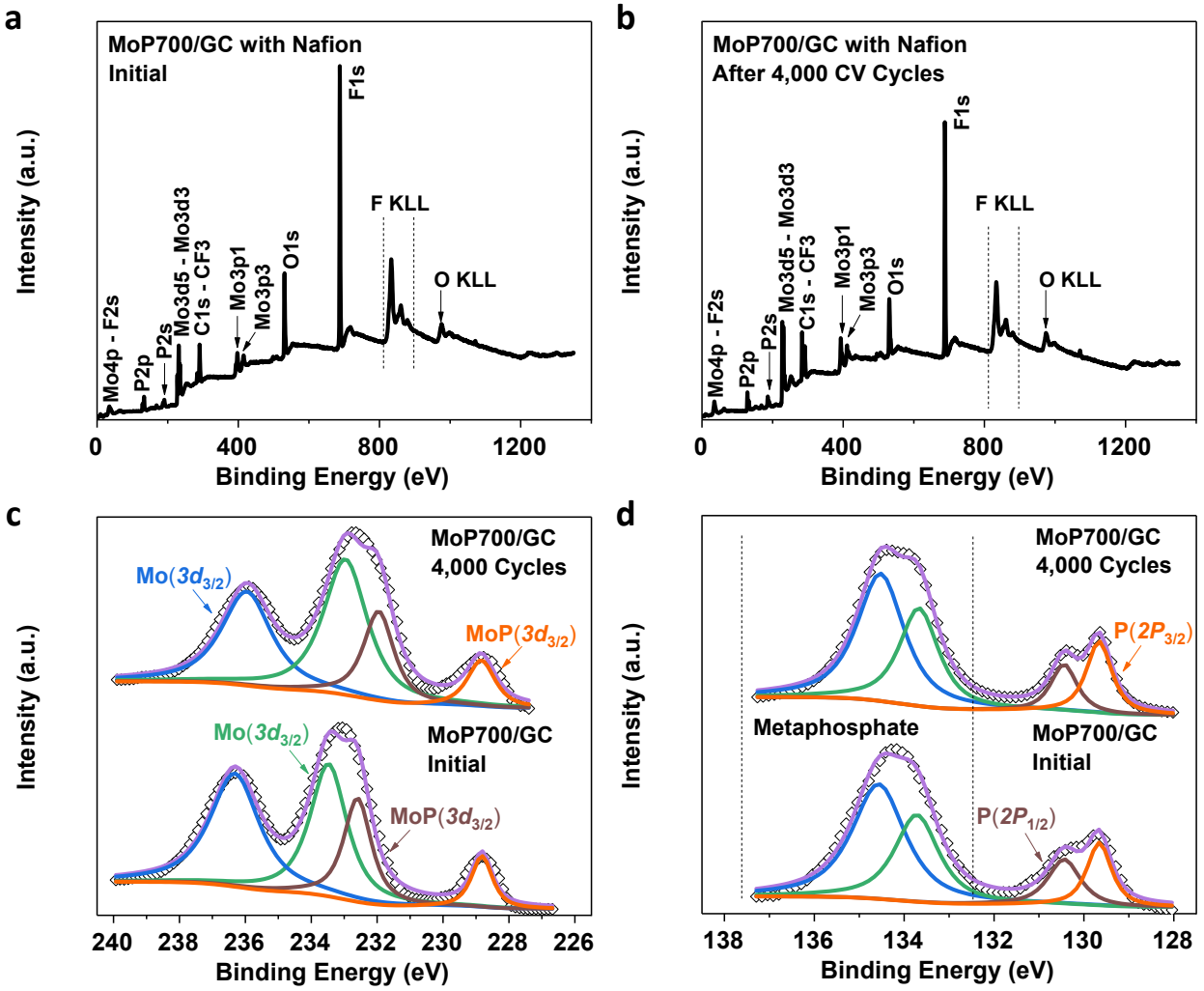

Figure S8.

XPS survey scan of MoP700/GC (a) before and (b) after 4,000 CV cycles between -0.45 and 0.15 V vs RHE in H_2-saturated 1.0 M PBS. XPS high resolution spectra of (c) Mo 3d and (d) P 2p before and after the stability tests, which indicates no obvious surface chemistry change during stability test.

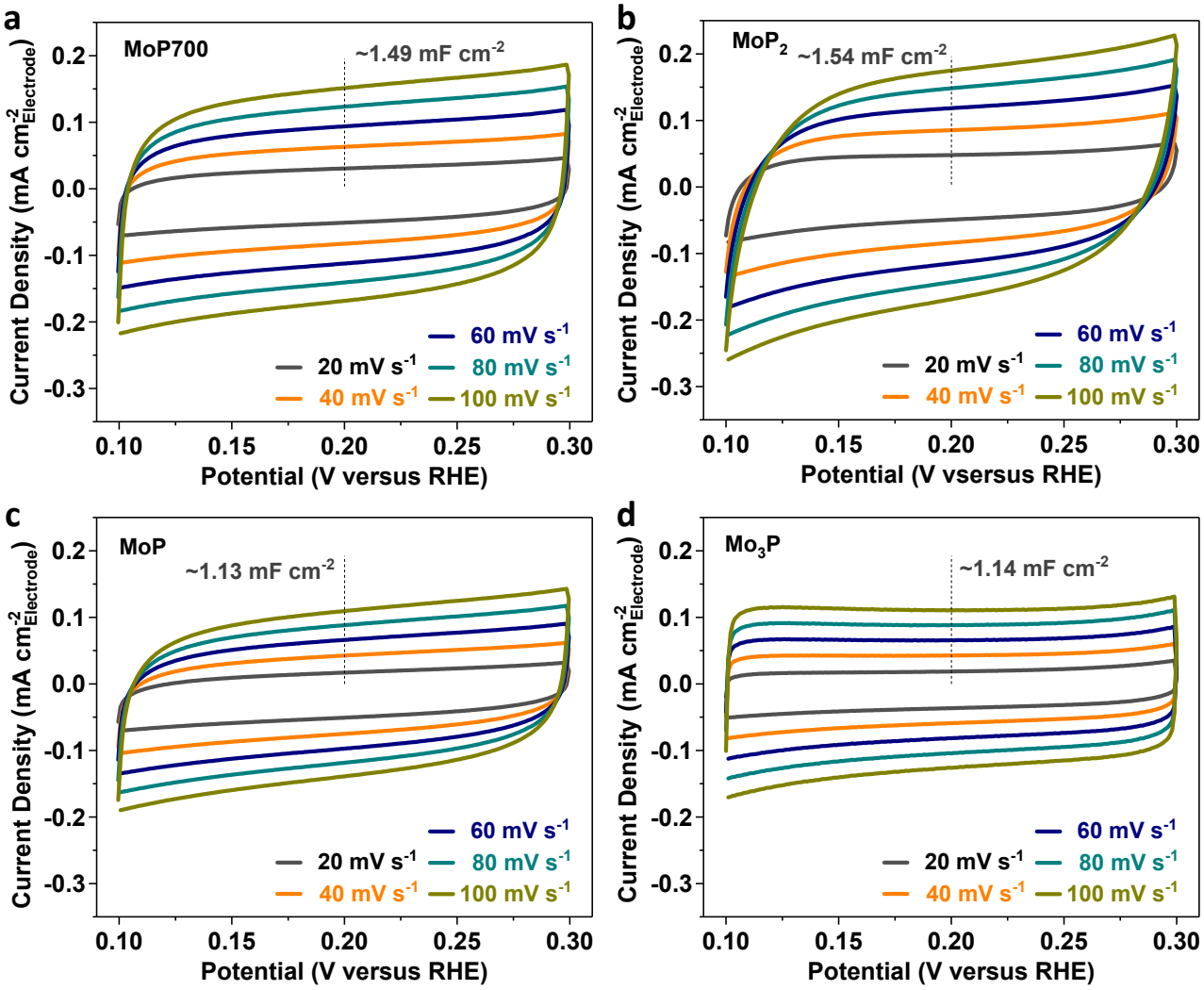

Figure S9.

CV curves of (a) MoP700, (b) MoP_2, (c) MoP and (d) Mo_3P in the potential region of 0.10-0.30 V (versus RHE) at various scan rate (20-100 mV s^{-1}).

The measured capacitive currents are used to determine the specific capacitance (C_{dl}) of electrodes ($\Delta J = ½(J_a - J_c)$ at 0.20 V against the scan rate).[5-7] The C_{dl} can be converted into an electrochemical surface area (A_{ECSA}) using the C_{dl} value for a flat standard with 1 cm^2 of real surface area. The C_{dl} for a flat surface is generally found to be in the range of 20-60 uF cm^{-2}.[8-9] In this work, we assume 40 uF cm^{-2}, which is a general practice in literature.[6-7] The A_{ECSA} of catalysts are calculated and presented in Figure S10.

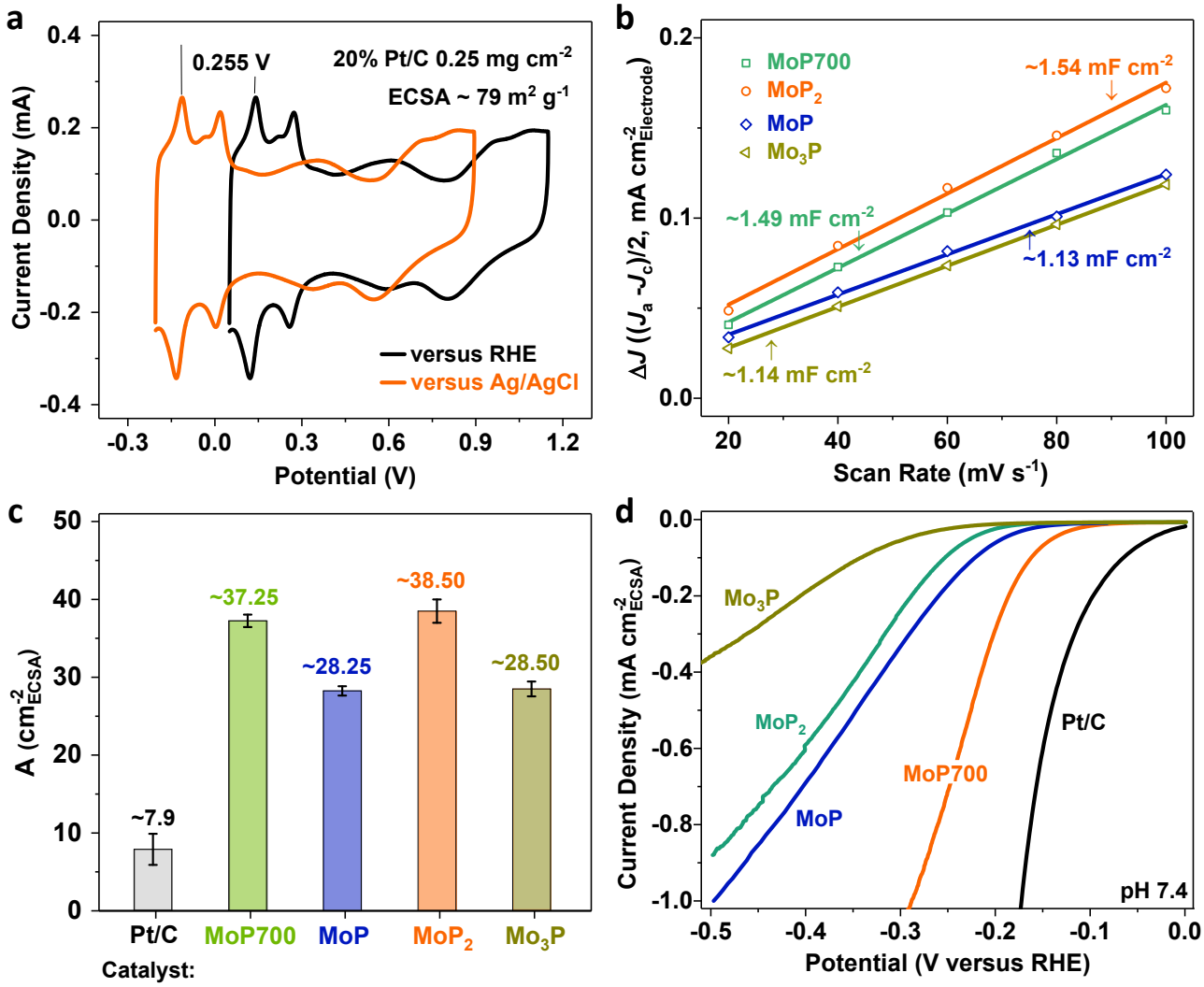

Figure S10.

(a) The calibration of Ag/AgCl (3.0M KCl) reference electrode with respect to reversible hydrogen potential using reversible hydrogen electrode (RHE) in H_2-saturated 0.5 M H_2SO_4; The calibration resulted in a shift of -0.255 V vs the RHE; thus, $E_{(RHE)} = 0.059\ pH + 0.255V$. (b) The measured C_{dl} (Figure S9) plotted as a function of scan rate. (c) Calculated A_{ECSA} for catalysts. (d) The measured HER polarization curves normalized to A_{ECSA}.

To calculate the A_{ECSA} of MoP_x and Pt catalysts (0.25 mg cm^{-2}) on electrodes, we use the following formula:[6-7]

$$A_{ECSA}^{Catalyst} = \frac{C_{dl}}{40\ \text{uF cm}^{-2}\ \text{per cm}^2_{ECSA}} \qquad A_{ECSA}^{Pt} = \frac{79\ m^2\ g^{-1}}{0.2 * 0.25\ \text{mg}\ cm^{-2} * 0.19625\ cm^2_{Electrode}}$$

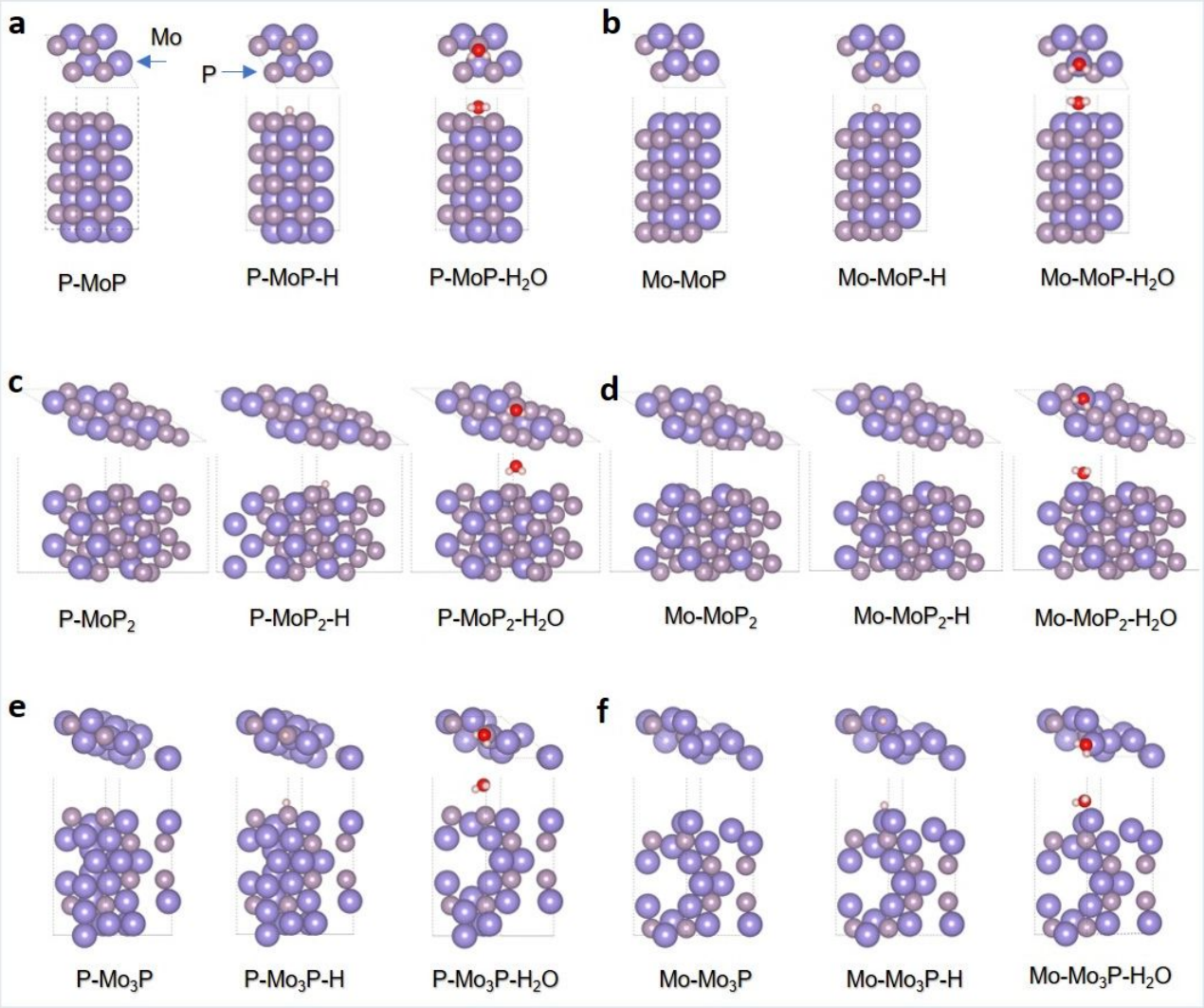

Figure S11.

Configuration of H and H_2O bind on (a) P-MoP, (b) Mo-MoP, (c) P-MoP_2, (d) Mo-MoP_2, (e) P-Mo_3P and (f) Mo-Mo_3P surfaces. P: pink, Mo: purple.

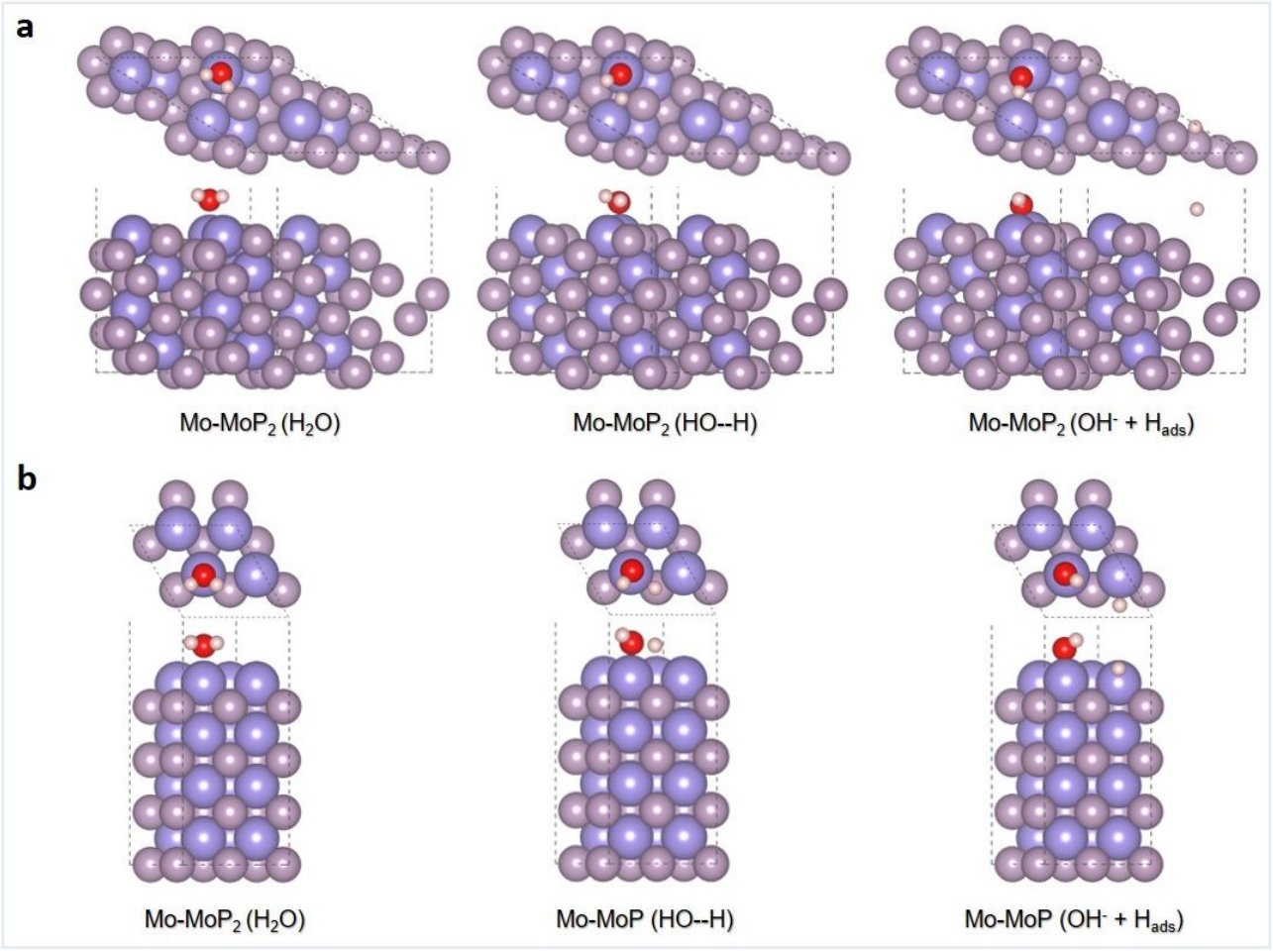

Figure S12.

Configuration of initial state, transition state and final state of H_2O dissociation reaction on the (a) Mo-MoP_2 and (b) Mo-MoP surfaces. P: pink, Mo: purple.

Table S1.
Comparison of the HER activity/performance of the MoP700 catalyst vis-à-vis some representative PGM-free HER electrocatalysts recently reported for 1.0 M PBS ([a] catalytic materials directly grown or attached on current collectors)

Catalyst	Loading (mg cm^{-2})	Current density (*j*) (mA cm^{-2})	η at the corresponding *j* (mV)	Reference
MoP700	0.25	10 25	196 245	This work
MoP NA/CC[a]	-	10	187	10
MoS_2/Mo[a]	-	10	244	11
MoP/CF[a]	-	1	300	12
MoB Mo_2C	-	1.5	315 241	13
Ni-S/FTO[a]		10	330	14
NiS_2 NA/CC	4.1(NiS_2)	10	243	15
MW-CoS	0.283	10	275	16

Table S2.
Comparison of the MEC activity/performance of the MoP700 catalyst vis-à-vis some representative electrocatalysts recently reported.

Optimal current density in MEC based on projected cathode surface (A m^{-2})	Catalyst type	Loading (mg cm^{-2})	Reference
157	MoP700	0.5	This work
145	Pt	0.5	
30	Electroformed Ni mesh	n/a	17
14	MoS_2	2.5	18
19	Stainless steel fiber felt	n/a	19
18	$Mg(OH)_2$/graphene	1.5	20

References

1 Duan HH, Li DG, Tang Y, He Y, Ji SF, Wang RY, et al. High-Performance Rh2P Electrocatalyst for Efficient Water Splitting. *J Am Chem Soc*. **2017**;*139(15)*:5494-502.

2 Wang MQ, Ye C, Xu MW, Bao SJ. MoP nanoparticles with a P-rich outermost atomic layer embedded in N-doped porous carbon nanofibers: Self-supported electrodes for efficient hydrogen generation. *Nano Res*. **2018**;*11(9)*:4728-34.

3 Oyama ST, Gott T, Zhao HY, Lee YK. Transition metal phosphide hydroprocessing catalysts: A review. *Catal Today*. **2009**;*143(1-2)*:94-107.

4 Shi YM, Zhang B. Recent advances in transition metal phosphide nanomaterials: synthesis and applications in hydrogen evolution reaction (vol 45, pg 1781, 2016). *Chem Soc Rev*. **2016**;*45(6)*:1781-.

5 Zhang HB, An PF, Zhou W, Guan BY, Zhang P, Dong JC, et al. Dynamic traction of lattice-confined platinum atoms into mesoporous carbon matrix for hydrogen evolution reaction. *Sci Adv*. **2018**;*4(1)*.

6 Kibsgaard J, Tsai C, Chan K, Benck JD, Norskov JK, Abild-Pedersen F, et al. Designing an improved transition metal phosphide catalyst for hydrogen evolution using experimental and theoretical trends. *Energ Environ Sci*. **2015**;*8(10)*:3022-9.

7 Kibsgaard J, Jaramillo TF. Molybdenum Phosphosulfide: An Active, Acid-Stable, Earth-Abundant Catalyst for the Hydrogen Evolution Reaction. *Angew Chem Int Edit*. **2014**;*53(52)*:14433-7.

8 Kotz R, Carlen M. Principles and applications of electrochemical capacitors. *Electrochim Acta*. **2000**;*45(15-16)*:2483-98.

9 Benck JD, Chen ZB, Kuritzky LY, Forman AJ, Jaramillo TF. Amorphous Molybdenum Sulfide Catalysts for Electrochemical Hydrogen Production: Insights into the Origin of their Catalytic Activity. *Acs Catal*. **2012**;*2(9)*:1916-23.

10 Pu ZH, Wei SY, Chen ZB, Mu SC. Flexible molybdenum phosphide nanosheet array electrodes for hydrogen evolution reaction in a wide pH range. *Appl Catal B-Environ*. **2016**;*196*:193-8.

11 Pu ZH, Liu Q, Asiri AM, Luo YL, Sun XP, He YQ. 3D macroporous MoS2 thin film: in situ hydrothermal preparation and application as a highly active hydrogen evolution electrocatalyst at all pH values. *Electrochim Acta*. **2015**;*168*:133-8.

12 Cui W, Liu Q, Xing ZC, Asiri AM, Alamry KA, Sun X. MoP nanosheets supported on biomass-derived carbon flake: One-step facile preparation and application as a novel high-active electrocatalyst toward hydrogen evolution reaction. *Appl Catal B-Environ*. **2015**;*164*:144-50.

13 Vrubel H, Hu XL. Molybdenum Boride and Carbide Catalyze Hydrogen Evolution in both Acidic and Basic Solutions. *Angew Chem Int Edit*. **2012**;*51(51)*:12703-6.

14 Jiang N, Bogoev L, Popova M, Gul S, Yano J, Sun YJ. Electrodeposited nickel-sulfide films as competent hydrogen evolution catalysts in neutral water. *J Mater Chem A*. **2014**;*2(45)*:19407-14.

15 Tang C, Pu ZH, Liu Q, Asiri AM, Sun XP. NiS2 nanosheets array grown on carbon cloth as an efficient 3D hydrogen evolution cathode. *Electrochim Acta*. **2015**;*153*:508-14.

16 You B, Jiang N, Sheng ML, Sun YJ. Microwave vs. solvothermal synthesis of hollow cobalt sulfide nanoprisms for electrocatalytic hydrogen evolution and supercapacitors. *Chem Commun*. **2015**;*51(20)*:4252-5.

17 Kadier A, Simayi Y, Chandrasekhar K, Ismail M, Kalil MS. Hydrogen gas production with an electroformed Ni mesh cathode catalysts in a single-chamber microbial electrolysis cell (MEC). *Int J Hydrogen Energ*. **2015**;*40(41)*:14095-103.

18 Tokash JC, Logan BE. Electrochemical evaluation of molybdenum disulfide as a catalyst for hydrogen evolution in microbial electrolysis cells. *Int J Hydrogen Energ*. **2011**;*36(16)*:9439-45.

19 Su M, Wei LL, Qiu ZZ, Wang G, Shen JQ. Hydrogen production in single chamber microbial electrolysis cells with stainless steel fiber felt cathodes. *J Power Sources*. **2016**;*301*:29-34.

20 Dai HY, Yang HM, Liu X, Jian X, Liang ZH. Electrochemical evaluation of nano-Mg(OH)(2)/graphene as a catalyst for hydrogen evolution in microbial electrolysis cell. *Fuel*. **2016**;*174*:251-6.